IEEE Access
Multidisciplinary | Rapid Review | Open Access Journal

Received May 13, 2020, accepted May 18, 2020, date of publication May 22, 2020, date of current version June 10, 2020.

Digital Object Identifier 10.1109/ACCESS.2020.2996753

Assessment of Model Predictive Voltage Control for Autonomous Four-Leg Inverter

RAEF ABOELSAUD[1,2], AMEENA SAAD AL-SUMAITI[3], AHMED IBRAHIM[1,2], IVAN V. ALEXANDROV[4], (Graduate Student Member, IEEE), ALEXANDER G. GARGANEEV[2], AND AHMED A. ZAKI DIAB[5]

[1]Department of Electrical Power and Machines Engineering, Zagazig University, Zagazig 44519, Egypt
[2]School of Energy and Power Engineering, National Research Tomsk Polytechnic University, 634050 Tomsk, Russia
[3]Advanced Power and Energy Center, Electrical Engineering and Computer Science Department, Khalifa University, Abu Dhabi, United Arab Emirates
[4]Department of Radio Engineering and Electronics, Novosibirsk State Technical University, 630073 Novosibirsk, Russia
[5]Electrical Engineering Department, Faculty of Engineering, Minia University, Minia 61111, Egypt

Corresponding authors: Raef Aboelsaud (rsahmed@eng.zu.edu.eg) and Ahmed A. Zaki Diab (a.diab@mu.edu.eg)

This work was supported by the Khalifa University, Abu Dhabi, United Arab Emirates, under Award FSU-2018-25.

ABSTRACT The Finite control set model predictive control (FCS-MPC) is recently introduced to control inverters without the modulation stage. The absence of the modulation stage gives an unpredictable performance of the control system. In this paper, the performance of FCS-MPC is assessed by comparing with PID control which is based on Scalar Pulse Width Modulation (PWM). The two control techniques are applied for load voltage regulation of the autonomous four-leg voltage source inverter (FLVSI). Practically, the predictive control requires a large number of calculations, resulting in high computation time and delay. In this paper, a new finite control set model predictive voltage control (MPVC) algorithm is proposed to predict the load voltages for 15 switching states instead of 16 switching states for reducing the computation time required for the control algorithm. Moreover, the algorithm is optimized by removing the repeated computations and the delay is compensated using the two-step prediction horizon principle. An accurate discrete-time state-space model of the autonomous FLVSI with output LC-filter is used for predicting the load voltages considering the neutral inductance and damping resistance of the LC filter. A simple PID control scheme with decoupled feedforward voltage and current loops is used in the DQ0 reference frame, while MPVC operates in the ABC reference frame. The simulation and experimental results are used to show the full assessment of the MPVC. The prominent outcomes show the ability of the proposed MPVC algorithm to provide high power quality under unbalanced and non-linear load conditions with high stability and robustness.

INDEX TERMS FCS-MPC, four-leg VSI, predictive voltage control, inverter, load unbalances, PWM, PID control, computation time reduction.

I. INTRODUCTION

Recently, power converters are considered as the main electric power components in providing good power quality in various electric power systems [1]. In Autonomous power supply systems (APS), the power generation is limited and the loads can be asymmetrical or non-linear. Low power quality issues have recently gained considerable attention due to its effects on electric and electronic equipment, such as overvoltage, vibration, overheating, and etc [2], [3].

The associate editor coordinating the review of this manuscript and approving it for publication was Jenny Mahoney.

For handling these issues, the three-phase four-leg voltage source inverter (FLVSI) is introduced. The fourth leg of this topology provides the neutral line, giving a high ability of per phase voltage control. This topology doesn't require large and high-cost DC link capacitors because the percentage ripple of DC link voltage is lower than that in the other inverter topologies. Furthermore, the FLVSI has found widespread applications, such as uninterruptible power supplies, electric vehicles, distributed generators, renewable power sources, active filters, micro-grids, and etc [4]–[9].

Recently, the Finite Control Set Model Predictive Control (FCS-MPC) is gaining a high interest in power electronic

applications due to its ability to deal with the discrete nature of the electronic devices, and its simple conception and implementation [10], [11]. Unlike the conventional control techniques, e.g. PID and PR control techniques, FCS-MPCý can control the inverter without modulation stage and has no need for parameter tuning. This control technique is away from the conventional control problems, such as the windup and the variables decoupling. Furthermore, the performance of the FCS-MPC can be flexibly adjusted by changing its objective and constraints in its control algorithm [12]–[15]. All these advantages enable the FCS-MPC to be an alternative tool to control the power converters.

Basically, the FCS-MPC control technique can be applied as a model predictive current control (MPCC) to control the output inverter current or as a model predictive voltage control (MPVC) for controlling the voltages of the loads connected to the inverters.

To assess the FCS-MPC performance, comparative analyses of MPVC and MPCC with the classical control techniques were carried out in the literature. MPCC is compared with PI control and hysteresis control for FLVSI [16] and three-leg VSI [17]. The work in [18] evaluates the robustness of MPCC against the deviation of system parameters in comparison with the PI control. In [19], MPVC performance is evaluated in comparison with carrier-based PWM for FLVSI. The comparative studies for MPVC in literature are lack of case studies under inductive loads, non-linear loads, transient conditions, and did not give a view of the f_s variation of the MPVC in the comparative analyses. All the mentioned gaps are assessed and discussed in this work. One of the main contributions of this work is to fill the gap in this research area.

The FCS-MPC technique has some drawbacks, such as: 1) The performance of the FCS-MPC depends on the accuracy of the system model. 2) Due to the absence of the modulation stage, the FCS-MPC operates under variable switching frequency (f_s); this affects the load harmonic spectrum and filter design. 3) The FCS-MPC requires a large number of calculations, resulting in high computation time (CT) for the algorithm implementation that requires high-speed microprocessors.

To mitigate the mentioned drawbacks, researches are presented in literature to improve the performance of the FCS-MPC. The work in [20] improves the MPVC robustness against model mismatches by using the Kalman filter-based observer. The work in [21] improves the steady-state performance of the MPVC by modifying the cost function to track both the voltage reference and its derivative simultaneously. A number of FCS-MPC algorithms are proposed in literature to reduce the switching frequency variation [22]. These Fixed switching frequency FCS-MPC algorithms require additional calculations which increase the time burden of the algorithms [23]. The Fixed switching frequency issue is not concerned in this paper.

It is well known that the FCS-MPC algorithm should be implemented in short sampling time to achieve the required control performance [24]. This is a significant challenge for the control realization due to the large number of calculations required for the FCS-MPC algorithm. The CT reduction of MPCC algorithm in [25] is based on avoiding the prediction of the voltage vectors that are far from the desired voltage vector, resulting in a reduction of the time required for the voltage prediction. This method is used only for T-type three-level inverter, which limits its applications. However, for the three-leg VSI, the method in [26] is based on selecting between only two switching states (SS)s instead of 8 SSs in the optimization problem of the MPCC algorithm. The control algorithm is implemented in the Simulink-Real-Time system with a high sampling period of 100 μs. In [27], a double-CPU, namely FPGA plus DSP controller, is employed to implement the MPCC algorithm in parallel calculations, so as to reduce its CT, without considering the CT reduction in the FCS-MPC algorithm itself. The CT issue of the MPVC is efficiently resolved in [28] by combining the MPVC with artificial Neural Networks but this method is not experimentally validated.

In this paper, a new MPVC algorithm is proposed to reduce its CT. In the proposed algorithm, the load voltage prediction is performed for 15 SSs instead of 16 SSs in the FLVSI connected with output LC-filter. Moreover, the algorithm is optimized by removing the repeated computations without affecting its performance. The proposed algorithm reduces the CT by 56% and can be experimentally implemented with minimum sampling time which is equal to 25 μs. Moreover, the optimization principle of the proposed MPVC algorithm is simple and can be applied for any inverter topology. The two-step prediction horizon principle, proposed in [29], is applied to compensate the time delay which can be induced in the MPVC algorithm implementation. As MPVC depends on the system model, an accurate system model is needed. Therefore, this algorithm uses a novel discrete-time model with considering the neutral inductance L_n and the damper resistance R_d of the LC-filter connected to the inverter. The performance of the MPVC is fully assessed by comparing it with PID control based PWM. The comparative study has been carried out to test the two control techniques in steady-state, and transient conditions. Moreover, the robustness analyses have been performed for the two control techniques against the load variations and system parameters deviations. The PID control scheme with two decoupling feedforward voltage and current loops in the DQ0 reference frame (SRF) is presented, while MPVC operates, in this paper, in the ABC reference frame (NRF).

Therefore, the contributions of this paper can be pointed out as follows:

1. A full assessment of the FCS-MPC as a voltage control in comparison with the conventional control technique (PID-control) with considering robustness analyses.
2. Accurate system model with considering L_n and R_d.

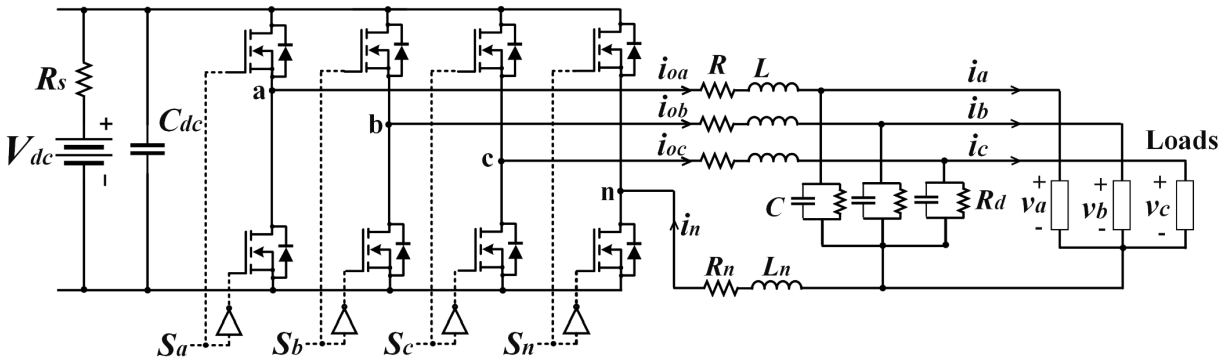

FIGURE 1. The FLVSI connected with LC-filter and loads.

3. Effective reduction of the CT of the control algorithm to be experimentally implemented with minimum sampling time.

The rest of the paper can be organized as follows. Section II elaborates on the discrete predictive modeling of the FLVSI. Section III describes the proposed MPVC algorithm. The stability analysis of MPVC is studied in section IV. Section V presents the scheme of the PID control. The simulation and experimental results considering the steady-state, transient, robustness, and stability analyses are presented in sections VI and VII. In conclusion, the research findings are recapitulated.

II. SYSTEM MODEL

The FLVSI topology in APS is depicted in Fig. 1. The LC-filter is used for filtering high order harmonics. The neutral inductor L_n is utilized to mitigate the oscillations of the neutral current [30]. A damping resistance R_d is added to improve the system stability at the resonance of the LC-filter [31]. The renewable power generation and storage systems of the autonomous power supply system can be replaced by an ideal DC voltage source V_{dc} with internal resistance R_s.

Generally, the FLVSI has 16 SSs. Every SS provides a certain output phase voltage as shown in Table 1. S_a, S_b, S_c, and S_n are the control signals of the upper switches. It can be noticed that the last two SSs in Table 1 provide zero vector states where the four legs are short-circuited. The output voltages can be expressed as follows:

$$e_{an} = (S_a - S_n)V_{dc}, \tag{1}$$
$$e_{bn} = (S_b - S_n)V_{dc}, \tag{2}$$
$$e_{cn} = (S_c - -S_n)V_{dc} \tag{3}$$

where V_{dc} is the input DC voltage. For simplification, the output inverter voltages, load voltages, output inverter current, and load currents, respectively, can be expressed in vectors as:

$$\mathbf{e} = \begin{bmatrix} e_{an} & e_{bn} & e_{cn} \end{bmatrix}^T, \tag{4}$$

TABLE 1. Switching states Of FLVSI with the corresponding output voltage.

	S_a	S_b	S_c	S_n	e_{an}	e_{bn}	e_{cn}
1	1	0	0	0	V_{dc}	0	0
2	0	1	0	0	0	V_{dc}	0
3	1	1	0	0	V_{dc}	V_{dc}	0
4	0	0	1	0	0	0	V_{dc}
5	1	0	1	0	V_{dc}	0	V_{dc}
6	0	1	1	0	0	V_{dc}	V_{dc}
7	1	1	1	0	V_{dc}	V_{dc}	V_{dc}
8	0	0	0	1	$-V_{dc}$	$-V_{dc}$	$-V_{dc}$
9	1	0	0	1	0	$-V_{dc}$	$-V_{dc}$
10	0	1	0	1	$-V_{dc}$	0	$-V_{dc}$
11	1	1	0	1	0	0	$-V_{dc}$
12	0	0	1	1	$-V_{dc}$	$-V_{dc}$	0
13	1	0	1	1	0	$-V_{dc}$	0
14	0	1	1	1	$-V_{dc}$	0	0
15	1	1	1	1	0	0	0
16	0	0	0	0	0	0	0

$$\boldsymbol{v} = \begin{bmatrix} v_a & v_b & v_c \end{bmatrix}^T, \tag{5}$$
$$\boldsymbol{i} = \begin{bmatrix} i_{oa} & i_{ob} & i_{oc} \end{bmatrix}^T, \tag{6}$$
$$\boldsymbol{i_L} = \begin{bmatrix} i_a & i_b & i_c \end{bmatrix}^T \tag{7}$$

Using differential equations, the system model can be derived as follows:

$$\boldsymbol{e} = R\boldsymbol{i} + L\frac{d\boldsymbol{i}}{dt} + \boldsymbol{v} + L_n\frac{di_n}{dt} + R_n i_n, \tag{8}$$
$$\boldsymbol{i} = \boldsymbol{i_L} + C\frac{d\boldsymbol{v}}{dt} + \boldsymbol{v}/R_d, \tag{9}$$
$$i_n = i_{oa} + i_{ob} + i_{oc} \tag{10}$$

By solving Eq. (8) and Eq. (9), this model can be represented in a state-space presentation as:

$$\frac{d}{dt}\begin{bmatrix} \boldsymbol{v} \\ \boldsymbol{i} \end{bmatrix} = \boldsymbol{A}\begin{bmatrix} \boldsymbol{v} \\ \boldsymbol{i} \end{bmatrix} + \boldsymbol{B}\begin{bmatrix} \boldsymbol{e} \\ \boldsymbol{i_L} \end{bmatrix} \tag{11}$$

where:

$$\boldsymbol{A} = \begin{bmatrix} -\boldsymbol{I}/R_d C & \boldsymbol{I}/C \\ -\boldsymbol{L_{eq}^{-1}} & -\boldsymbol{L_{eq}^{-1}}\boldsymbol{R_{eq}} \end{bmatrix}_{6\times 6},$$
$$\boldsymbol{B} = \begin{bmatrix} \boldsymbol{0} & -\boldsymbol{I}/C \\ \boldsymbol{L_{eq}^{-1}} & \boldsymbol{0} \end{bmatrix}_{6\times 6}, \tag{12}$$

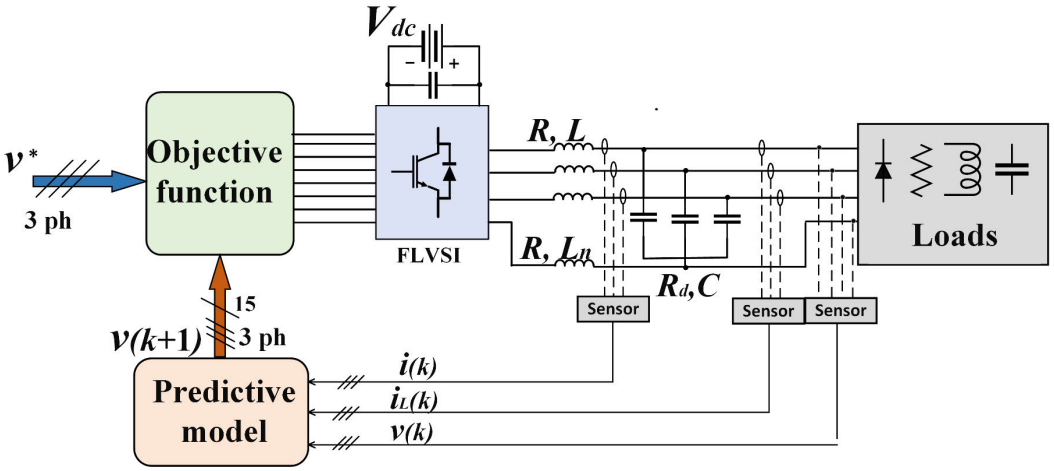

FIGURE 2. Block diagram of FLVSI controlled by MPVC.

$$\boldsymbol{L_{eq}} = \begin{bmatrix} 2 & 1 & 1 \\ 1 & 2 & 1 \\ 1 & 1 & 2 \end{bmatrix} \times L, \quad \boldsymbol{R_{eq}} = \begin{bmatrix} 2 & 1 & 1 \\ 1 & 2 & 1 \\ 1 & 1 & 2 \end{bmatrix} \times R \tag{13}$$

where $\boldsymbol{0}$ and $\boldsymbol{I}$ are third-order zero and unit matrices, respectively. In this paper, the filter and the neutral line inductances are assumed to be equal ($L_n = L$ and $R_n = R$). From the continuous state-space model in Eq. (11), the discrete system model can be derived as follows:

$$\begin{bmatrix} \boldsymbol{v}(k+1) \\ \boldsymbol{i}(k+1) \end{bmatrix} = \boldsymbol{Q} \begin{bmatrix} \boldsymbol{v}(k) \\ \boldsymbol{i}(k) \end{bmatrix} + J \begin{bmatrix} \boldsymbol{e} \\ \boldsymbol{i_L}(k) \end{bmatrix} \tag{14}$$

where:

$$\boldsymbol{Q} = \begin{bmatrix} q_1 & q_2 \\ q_3 & q_4 \end{bmatrix} = exp\,\{\boldsymbol{A}T_s\} \tag{15}$$

$$\boldsymbol{J} = \begin{bmatrix} j_1 & j_2 \\ j_3 & j_4 \end{bmatrix} = \boldsymbol{A}^{-1}(\boldsymbol{Q} - \boldsymbol{I}_{6\times6})\boldsymbol{B} \tag{16}$$

T_s is the sampling time, and k is the discrete sampling instant. From the discrete system model in (14), the predicted load voltage vector can be obtained for each SS as following:

$$\boldsymbol{v}(k+1) = q_1\boldsymbol{v}(k) + q_2\boldsymbol{i}(k) + j_1\boldsymbol{e} + j_2\boldsymbol{i_L} \tag{17}$$

For each SS, $\boldsymbol{e}$ has a new value according to Table 1, consequently the predicted load voltage has different values for the 16 SSs.

III. PREDICTIVE VOLTAGE CONTROL ALGORITHM

The block diagram of the FLVSI controlled by MPVC approach is shown in Fig. 2. The algorithm of the MPVC can be briefly described in the following steps:

- Measure the load voltage, load current, output current vectors.
- Predicted the load voltage for each SS using eq. (17)
- Evaluate the objective function (g) is calculated for each given predicted value of the load voltage

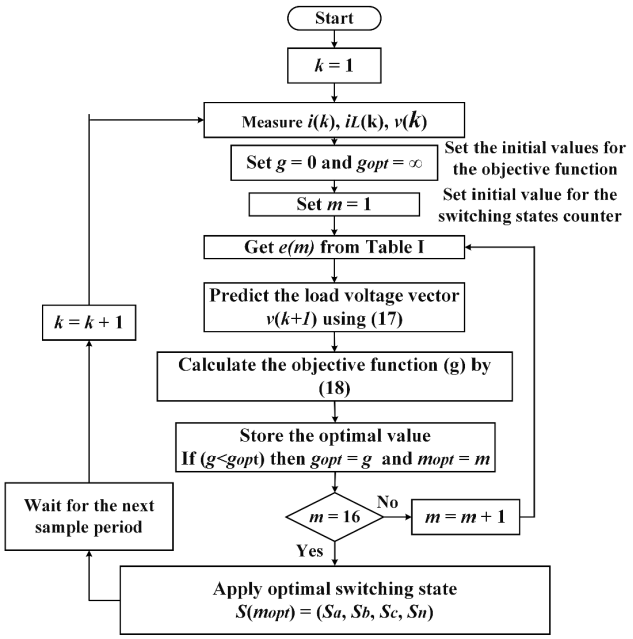

FIGURE 3. Flowchart of the MPVC algorithm.

- Select the best SS that gives the minimum value of the objective function;
- Finally, the selected SS is applied to the FLVSI switches. This algorithm is performed for each sampling interval using the flowchart depicted in Fig. 3.

The objective function can be defined as follows:

$$g = (v_a^* - v_a(k+1))^2 + (v_b^* - v_b(k+1))^2 + (v_c^* - v_c(k+1))^2 \tag{18}$$

where v_a^*, v_b^*,v_c^* are the reference phase voltage. $v_a(k+1)$ $v_b(k+1)$, $v_c(k+1)$ are the predicted load voltages which are derived from the discrete system model. The objective function is the error between the reference and the predicted value

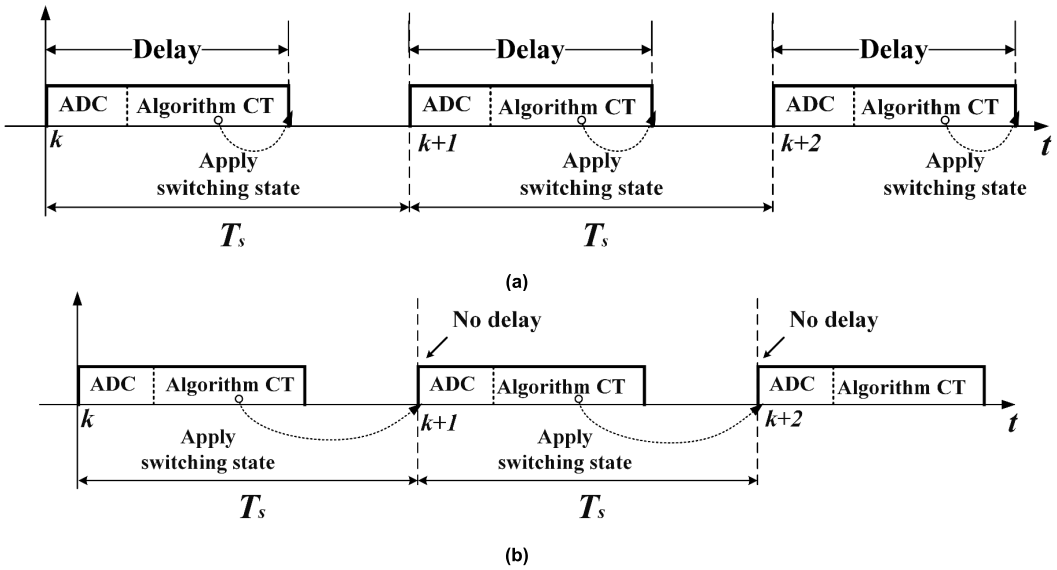

FIGURE 4. Timeline of control system based FCS-MPC for each sampling period in case of (a) one-step prediction horizon (b) two-step prediction horizo.

of the load voltage. The MPVC will be in NRF to control the load voltages independently.

A. TWO-STEP PREDICTION HORIZON FOR DELAY COMPENSATION

In practical implementation, a delay time is provided by the sensors and the analog to digital converters (ADC) which are used to measure the required signals for the control algorithm. After the measurement procedure, the control algorithm requires a CT to perform a number of calculations to apply the new SS. Therefore, there will be a significant delay between the starting of the signal measurement and the instant of application of the new SS, as shown in Fig. 4a, resulting in high harmonic distortions in the controlled signals.

To compensate this delay, the two-step prediction horizon principle proposed for the MPCC in [29] will be applied for the proposed algorithm. This compensation is based on predicting the load voltage for two-step prediction $(k+2)$, and the chosen SS will not be applied in the current interval but at the beginning of the next sampling period, as shown in Fig. 4b. In this way, the control algorithm is modified as follows:

1- Start the sensing and ADC procedure.
2- While the ADC procedure is running, apply the SS which is calculated in the previous sampling period.
3- Calculate the load current for the next sampling period using the Lagrange extrapolation method:

$$i_{\boldsymbol{L}}(k+1) = 4\, i_{\boldsymbol{L}}(k) - 6 i_{\boldsymbol{L}}(k-1) + 4 i_{\boldsymbol{L}}(k-2) - i_{\boldsymbol{L}}(k-3)(19) \quad (19)$$

4- Predict the load voltage and output inverter current for two-step prediction horizon as follows:

$$\begin{bmatrix} \boldsymbol{v}(k+2) \\ \boldsymbol{i}(k+2) \end{bmatrix} = \boldsymbol{Q} \begin{bmatrix} \boldsymbol{v}(k+1) \\ \boldsymbol{i}(k+1) \end{bmatrix} + \boldsymbol{J} \begin{bmatrix} \boldsymbol{e} \\ \boldsymbol{i_L}(k+1) \end{bmatrix} \quad (20)$$

where $\boldsymbol{v}(k+1)$ and $\boldsymbol{i}(k+1)$ are the predicted load voltage and inverter current which are calculated in the previous interval.

5- Select the best SS according to the following objective function:

$$g = \left[v_a^* - v_a\,(k+2)\right]^2 + \left[v_b^* - v_b\,(k+2)\right]^2 + \left[v_c^* - v_c\,(k+2)\right]^2 \quad (21)$$

B. THE OPTIMIZED MPVC ALGORITHM

It is the fact that with decreasing the sampling time (T_s), the FCS-MPC algorithm shows better performance. To decrease T_s, high-speed microcontrollers are required to perform a large number of calculations in lower time, resulting in high cost. On the other hand, the MPVC algorithm can be optimized to reduce its CT without affecting its performance or changing the available microprocessor. Firstly, the control algorithm will search in 15 SSs instead of 16 SSs by combining the two zero vector states (15th and 16th SS in Table 1) in one zero vector state and choose between them randomly, as shown in Fig. 5.

Secondly, some calculations in the voltage prediction don't need to be performed for every SS. To optimize the time required for the voltage predictions, eq. (17) can be rewritten as:

$$\boldsymbol{v}(k+2) = \begin{bmatrix} v_a(k+2) \\ v_b(k+2) \\ v_c(k+2) \end{bmatrix} = \boldsymbol{Q_v} + j_1 \boldsymbol{e} \quad (22)$$

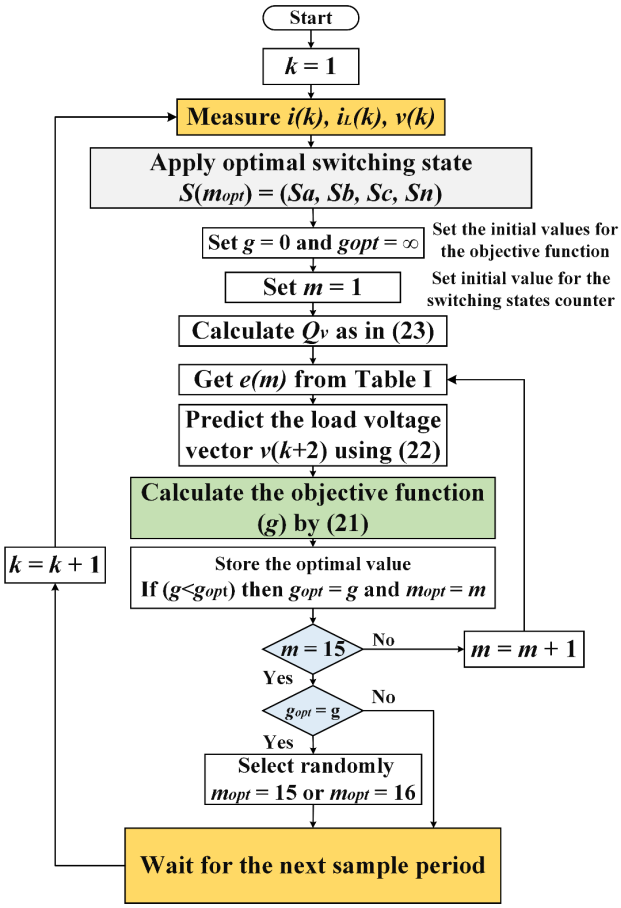

FIGURE 5. Flowchart of the proposed MPVC algorithm.

where:

$$\boldsymbol{Q_v} = \begin{bmatrix} Q_{va} \\ Q_{vb} \\ Q_{vc} \end{bmatrix} = q_1 \boldsymbol{v}(k+1) + q_2 \boldsymbol{i}(k+1) + j_2 \boldsymbol{i_L}(k+1) \quad (23)$$

$\boldsymbol{Q_v}$ is calculated only for one time every sampling interval. However, the MPVC algorithms in Fig. 3 and Fig 5 show the same performance in simulation because they are ideally simulated. The proposed MPVC algorithm has the superiority to be practically implemented.

IV. PID CONTROL STRUCTURE

The PID control is a classic linear control, which is widely used in power electronic applications. In this work, the PID control scheme is developed to control the FLVSI. This control operates in the SRF to regulate the controllable variables in the DC condition. This scheme consists of an outer voltage control loop to regulate the load voltages and inner current control loops to provide the control commands for the scalar PWM. To enhance the PID control reliability, the coupling between the D and Q coordinates is compensated by using decoupling feedforward voltage and current loops as shown in Fig 6.

To transformation of the system variables from NRF to SRF reference frame can be expressed as:

$$\begin{bmatrix} e_d \\ e_q \\ e_0 \end{bmatrix} = \boldsymbol{T} \begin{bmatrix} e_{an} \\ e_{bn} \\ e_{cn} \end{bmatrix}, \quad \begin{bmatrix} v_d \\ v_q \\ v_0 \end{bmatrix} = \boldsymbol{T} \begin{bmatrix} v_a \\ v_b \\ v_c \end{bmatrix}, \quad (24)$$

$$\begin{bmatrix} i_d \\ i_q \\ i_0 \end{bmatrix} = \boldsymbol{T} \begin{bmatrix} i_{oa} \\ i_{ob} \\ i_{oc} \end{bmatrix}, \quad \begin{bmatrix} i_{Ld} \\ i_{Lq} \\ i_{L0} \end{bmatrix} = \boldsymbol{T} \begin{bmatrix} i_a \\ i_b \\ i_c \end{bmatrix} \quad (25)$$

where:

$$T = \frac{2}{3} \begin{bmatrix} \cos(\omega t) & \cos(\omega t - 2\pi/3) & \cos(\omega t + 2\pi/3) \\ -\sin(\omega t) & -\sin(\omega t - 2\pi/3) & -\sin(\omega t + 2\pi/3) \\ 1/2 & 1/2 & 1/2 \end{bmatrix}, \quad (26)$$

where ω is the angular frequency. The system model in the SRF is presented as follows:

$$\begin{bmatrix} e_d \\ e_q \\ e_0 \end{bmatrix} = 2R \begin{bmatrix} i_d \\ i_q \\ i_0 \end{bmatrix} + 2L \frac{d}{dt} \begin{bmatrix} i_d \\ i_q \\ i_0 \end{bmatrix} + \omega L \begin{bmatrix} -i_q \\ i_d \\ 0 \end{bmatrix} + \begin{bmatrix} v_d \\ v_q \\ v_0 \end{bmatrix}, \quad (27)$$

$$\begin{bmatrix} i_d \\ i_q \\ i_0 \end{bmatrix} = \begin{bmatrix} i_{Ld} \\ i_{Lq} \\ i_{L0} \end{bmatrix} + C \frac{d}{dt} \begin{bmatrix} v_d \\ v_q \\ v_0 \end{bmatrix} + \begin{bmatrix} v_d \\ v_q \\ v_0 \end{bmatrix} / R_d + \omega C \begin{bmatrix} -v_q \\ v_d \\ 0 \end{bmatrix} \quad (28)$$

where ωL and ωC are the cross-coupling terms between D and Q axes in the SRF.

V. CURRENT CONTROL LOOP

From Eq. (27), the voltage drop between the inverter and loads can be presented as:

$$\begin{bmatrix} v_{fd} \\ v_{fq} \\ v_{f0} \end{bmatrix} = 2R \begin{bmatrix} i_d \\ i_q \\ i_0 \end{bmatrix} + 2L \frac{d}{dt} \begin{bmatrix} i_d \\ i_q \\ i_0 \end{bmatrix}, \quad (29)$$

The PID controller, in the current control loop, can be used to regulate the voltage drop basing on inductor current feedback, i.e.

$$\begin{bmatrix} v_{fd} \\ v_{fq} \\ v_{f0} \end{bmatrix} = \left(k_p + k_i/s + k_d s\right) \begin{bmatrix} i_d^* - i_d \\ i_q^* - i_q \\ i_0^* - i_0 \end{bmatrix}, \quad (30)$$

where i_d^*, i_q^* and i_0^* are reference values for the inverter output currents. The eq. (27) can be rewritten using eq (30) as:

$$\begin{bmatrix} e_q \\ e_d \\ e_0 \end{bmatrix} = (k_p + k_i/s + k_d s) \begin{bmatrix} i_d^* - i_d \\ i_q^* - i_q \\ i_0^* - i_0 \end{bmatrix} + \omega L \begin{bmatrix} -iq \\ id \\ 0 \end{bmatrix} + \begin{bmatrix} v_q \\ v_d \\ v_0 \end{bmatrix}, \quad (31)$$

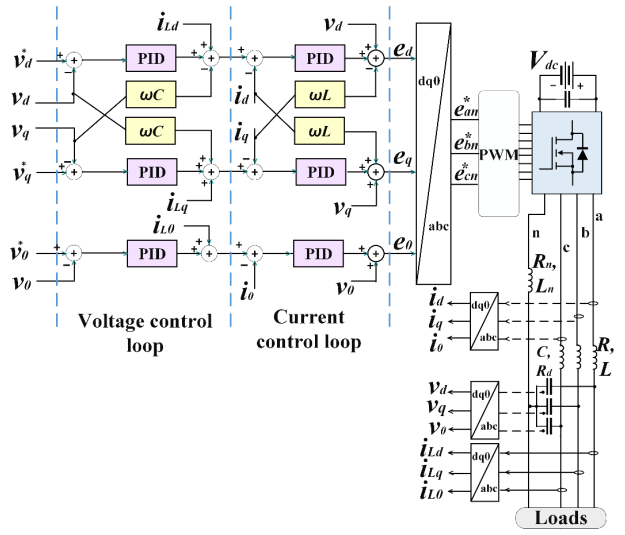

FIGURE 6. Schematic diagram of APS with the PID-controller.

A. VOLTAGE CONTROL LOOP

In the voltage control loop, the PID-controller can be applied to provide the references for the current in the shunt element of the LC-filter according to the load voltage feedback:

$$C\frac{d}{dt}\begin{bmatrix} v_d \\ v_q \\ v_0 \end{bmatrix} + \begin{bmatrix} v_d \\ v_q \\ v_0 \end{bmatrix} /R_d = \left(k_{pv} + k_{iv}/s + k_{dv}s\right)\begin{bmatrix} v_d^* - v_d \\ v_q^* - v_q \\ v_0^* - v_0 \end{bmatrix} \tag{32}$$

where v_d^*, v_q^* and v_0^* are the reference values for load voltages. By substituting Eq. (32) in Eq. (28), we have:

$$\begin{bmatrix} i_d^* \\ i_d^* \\ i_0^* \end{bmatrix} = \begin{bmatrix} i_{Ld} \\ i_{Lq} \\ i_{L0} \end{bmatrix} + \left(k_p + k_i/s + k_d s\right)\begin{bmatrix} v_d^* - v_d \\ v_q^* - v_q \\ v_0^* - v_0 \end{bmatrix} + \omega C \begin{bmatrix} -v_q \\ v_d \\ 0 \end{bmatrix} \tag{33}$$

By using equations (31) and (33), the block diagram of the APS with the PID control scheme can be depicted in Fig. 6. As shown in Fig. 6, the output signals of the current control loop (e_d, e_q, and e_0) are transferred to the NRF and applied to the scalar PWM which is sufficiently described in [32].

VI. STABILITY ANALYSIS OF THE PREDICTIVE CONTROL

The stability analysis used for MPCC in [33], [34] is employed in this work to validate the stability of the proposed MPVC. The block diagram of the APS with MPVC control system is depicted in Fig. 7a. The impedance of the load is represented by Z_L. The first-order transfer function of MPVC can be presented by the time constant (T_{eq}) and the gain (K_{MPVC}). The time constant corresponds to the equivalent time delays of the control algorithm execution and ADC, the time constant can be expressed by $T_{eq} = 0.85T_s$ [33]. The gain K_{MPC} can be defined by the amplitude ratio of the

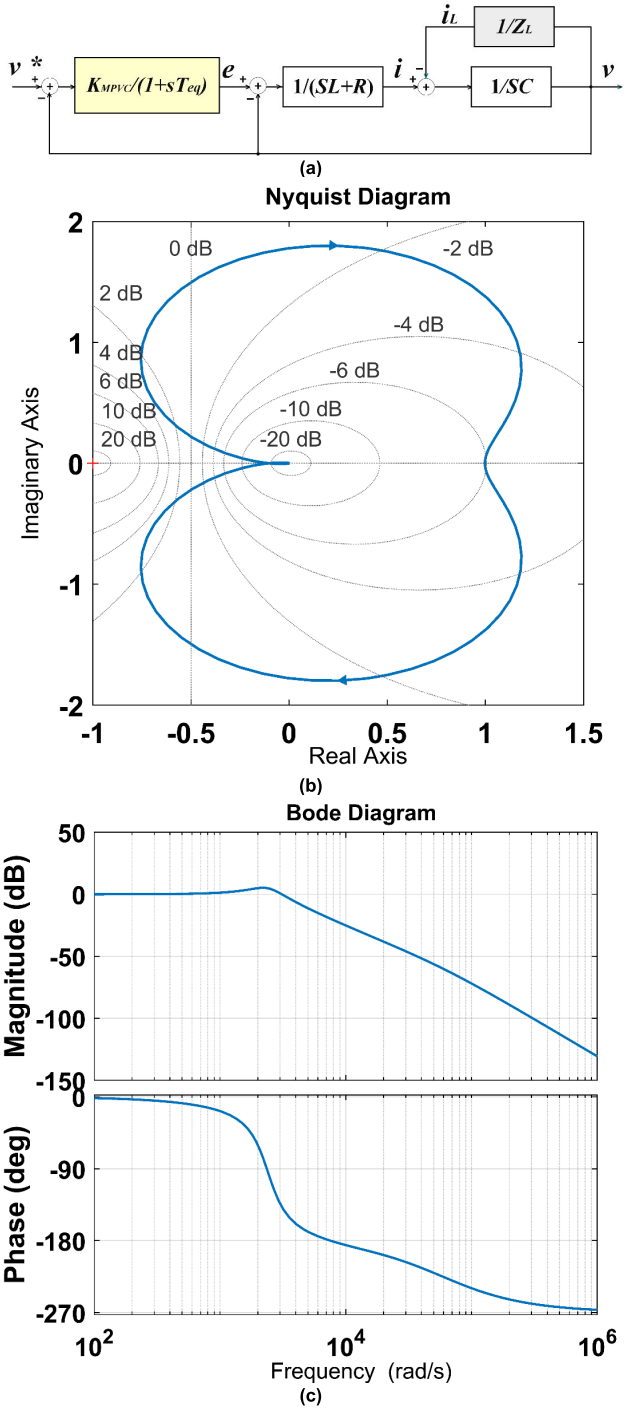

FIGURE 7. APS with MPVC (a) A simplified block diagram(b) Nyquist diagram (c) Bode diagram.

measured and reference voltages and is considered as a unity. The LC-filter parameters and load impedance are presented in Table 2.

The Nyquist criterion and Bode plot are employed to validate the stability of the control system. Fig. 7b shows a Nyquist plot of the open-loop transfer function of the system where the path is in the clockwise direction and located at the right half of the axis s $= -1$ which ensures the closed-loop

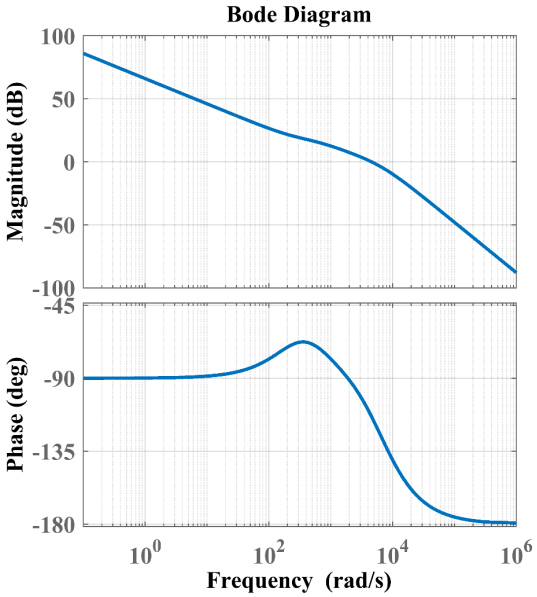

FIGURE 8. Bode diagram of APS with PID.

TABLE 2. System parameters.

Parameters	Values
DC input voltage of the inverter	V_{dc} = 640 V
The internal resistance of the input source	R_s = 0.25 Ω
Sampling time	T_s = 20 µs
DC-link capacitance	C_{dc} = 1000 µF
LC-filter	L = 2.5 mH, C= 80 µF, R = 0.02 Ω, Rd = 150 Ω
Standard Load impedance	Z_L: R_L = 10Ω, L_L = 1 mH

stability of the system. The Bode diagram is shown in Fig. 7c which reveals the stability of the system with a phase margin of 68 degrees.

To check the relative stability of the MPVC algorithm in comparison with the PID control, the phase margin of the system with the PID control is estimated using the bode diagram shown in Fig. 8. The PID control design and tuning is discussed exhasivly in []. The phase margin of the PID control is 66.5 degree which is slightly lower than those of the MPVC; this reveals that the relative stability of the MPVC is higher than PID control.

VII. SIMULATION RESULTS

The assessment of the MPVC is performed in MATLAB / SIMULINK software by comparing its performance with the PID control scheme. Three analyses are carried out: 1) steady-state 2) transient 3) robustness against load and parameters variations. The system parameters are listed in Table 2.

A. STEADY-STATE PERFORMANCE

Five load cases are applied in the steady-state mode:

TABLE 3. Load parameters.

Case	Load impedance
1) Balanced resistive load	$R_a = R_b = R_c$ = 15 Ω
2) Balanced inductive load	$R_a = R_b = R_c$ = 10 Ω $L_a = L_b = L_c$ = 20 mH
3) Unbalanced resistive load	R_a = 5Ω, R_b = 10Ω, Rc = ∞
4) Unbalanced inductive load	R_a = 5Ω, R_b = 10Ω, Rc = ∞ L_a = 10mH, L_b = 30mH
5) Non-linear unbalanced load	L_a' = 50 mH, R_a'=20 Ω, R_{b1}'=1 Ω, R_{b2}'=60 Ω, $C_{b'}$=3000 µF, L_c'= 20 mH, R_c'=70 Ω, C_c'= 5000 µF

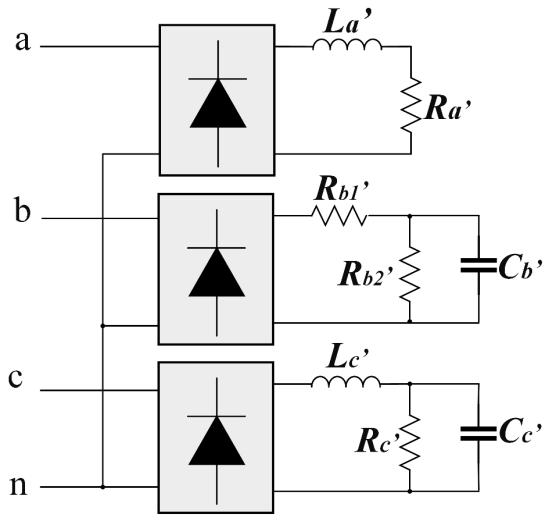

FIGURE 9. The topology of the three-phase non-linear unbalanced loads.

1) Three-phase balanced resistive load;
2) Three-phase balanced inductive load;
3) Three-phase unbalanced resistive;
4) Three-phase unbalanced inductive load;
5) Three-phase unbalanced nonlinear loads as depicted in Fig. 9.

The parameters of the mentioned load conditions are given in Table 3.

The load voltages, the load currents, and the DC-link voltage under the five load conditions are shown in Fig. 10. To assess the performance of the control techniques, the %THD of the load voltages, the voltage ripple in the DC link (% ΔV_{dc}), the phase voltage unbalance factor (PVUF) [35] and switching frequency (f_s) are used as performance indexes and evaluated for all load cases as shown in Table 4.

It can be observed that the MPVC and PID control can regulate the load voltage with low harmonic distortion for symmetrical, asymmetrical and nonlinear loads.

Compared to PID control, the MPVC provides lower harmonic distortion under resistive load conditions; the total harmonic distortion (%THD) is lower than 1%. The %THD with MPVC is higher in the case of inductive and non-linear

TABLE 4. Comparative analysis with PID control.

Case	MPVC						PID control					
	f_s (Hz)	% ΔVdc	THD			% PVUF	f_s (Hz)	% ΔVdc	THD			% PVUF
			Φa	Φb	Φc				Φa	Φb	Φc	
1	3754	0.3248	1.01	1.01	1.01	0.2248	4000	0.2004	1.29	1.3	1.26	0.1815
2	2071	0.6160	3.2	3.2	3.2	0.9592	4000	0.1971	1.4	1.4	1.4	0.1524
3	3968	1.7164	0.76	0.96	0.96	0.2007	4000	1.5411	1.45	1.47	1.44	0.1218
4	2177	1.6084	3.74	3.36	3.74	1.8977	4000	1.0109	1.49	1.48	1.45	0.3219
5	2436	0.8668	2.13	2.06	2.35	0.9426	4000	0.7095	1.62	1.5	1.54	0.0575

TABLE 5. Comparative analysis with MPVC presented in [37].

Load condition	MPVC algorithm	% THD			e_v(V)			U_f(V)		
		Φ_a	Φ_b	Φ_c	Φ_a	Φ_b	Φ_c	Φ_a	Φ_b	Φ_c
Case 1	Proposed	0.85	0.85	0.84	1.3774	1.2966	1.3172	309	309.2	309.1
	[37]	1.10	1.05	1.07	2.9364	2.9354	2.9354	309.4	309.4	309.2
Case 2	Proposed	1.34	1.34	1.18	2.1212	2.1755	2.0028	308.1	308	308.2
	[37]	1.55	1.74	1.70	4.3647	4.2601	4.2601	307.8	307.6	307.6
Case 3	Proposed	1.76	1.72	1.76	2.5589	2.6846	2.6805	307.4	307.2	307.2
	[37]	2.34	2.32	2.15	6.5723	6.4987	6.4987	305.6	305.7	306.7

loads, but not more than 4%. This may be due to the delaying behavior of the inductive current which reduces the prediction accuracy of the load voltage.

The % ΔV_{dc} is a significant factor for designing the DC-link capacitor [36]. Higher % ΔV_{dc} requires a larger DC-link capacitor, and consequently higher cost is required. However, the % ΔV_{dc} is higher in MPVC than PID control for all case studies, due to the f_s variation of MPVC. The difference in % ΔV_{dc} between MPVC and PID-control is small which is more evident in Fig. 12b. The PVUF value is lower than 2% for both control techniques. It is noticed that the PVUF is lightly higher with MPVC than with PID control under all load conditions.

An additional comparison is performed between the proposed MPVC algorithm and the simulation results presented in the [37] and enlisted in Table 5. To attain fair comparison, the LC-filter parameters, the DC-link voltage, the overall DC-link capacitance, and the three load cases given in [37] are considered in this study. The comparison is applied according to the evaluation criteria presented in [37] which are the %THD, the error between the RMS values of the load voltage and its reference (e_v), and the amplitude of the fundamental voltage (U_f). However, the inverter topology used in [37] is a three-level VSI. The two-level FLVSI provides lower %THD due to the accurate model employed in the proposed predictive voltage control algorithm. Moreover, the proposed algorithm has higher U_f values and lower e_v than that in [37]; this shows that the proposed algorithm has a higher ability of reference tracking.

B. TRANSIENT PERFORMANCE

Fig. 11 shows the load voltages and currents for MPVC and PID control at the moment of step-change from no-load to a resistive load ($R_a = R_b = R_c = 10\ \Omega$). The results show that the MPVC provides a faster dynamic response, compared to PID control. The settling time of this step response is 3 ms in MPVC, while in PID-controller the settling time of the step response is 4 ms. It can be noted that the fast transient performance of the MPVC is possible due to the absence of the modulation stage. In no-load condition, the MPVC provides higher THD than PID. Therefore, there are some oscillations at the transient period of the MPVC.

C. ROBUSTNESS ANALYSES

Two robustness tests are tested to appraise the effect of load variation and the change of LC-filter parameters on the proposed MPVC and PID control performance. The evaluation criterions of these tests are the average %THD, $\%\Delta V_{dc}$, and f_s. In the robustness test against the load variation, the load active power demand changes from zero Watt to 80 kW with a step change of one kW in four cases of unity, 0.9, 0.8 and 0.7 power factor. For the second robustness test, the filter inductance is ranged from 1.5 to 3.5 mH with a step change of 0.2 mH and the filter capacitance from 50 to 100 μF with a step change of 5 μF. It can be noted that the load parameters are not considered in the proposed predictive model, whereas the standard impedance of the load is considered in the PID control design which is ($R_L = 10\ \Omega$, $L_L = 1$ mH). Moreover, the predictive model and PID controller recognized the standard value of the LC-filter parameters which are 2.5 mH and 80 μF.

Fig. 12a shows the %THD variation with changing load power and power factor for MPVC and PID. The deviation of %THD from no-load to high load is lower in MPVC than that in PID under various power factors. It can be indicated that the proposed MPVC has more robustness against load variations than PID. The $\%\Delta V_{dc}$ variation for MPVC and PID control under load change is shown in Fig. 12b. The load variation has a little impact on the $\%\Delta V_{dc}$ for the two control techniques.

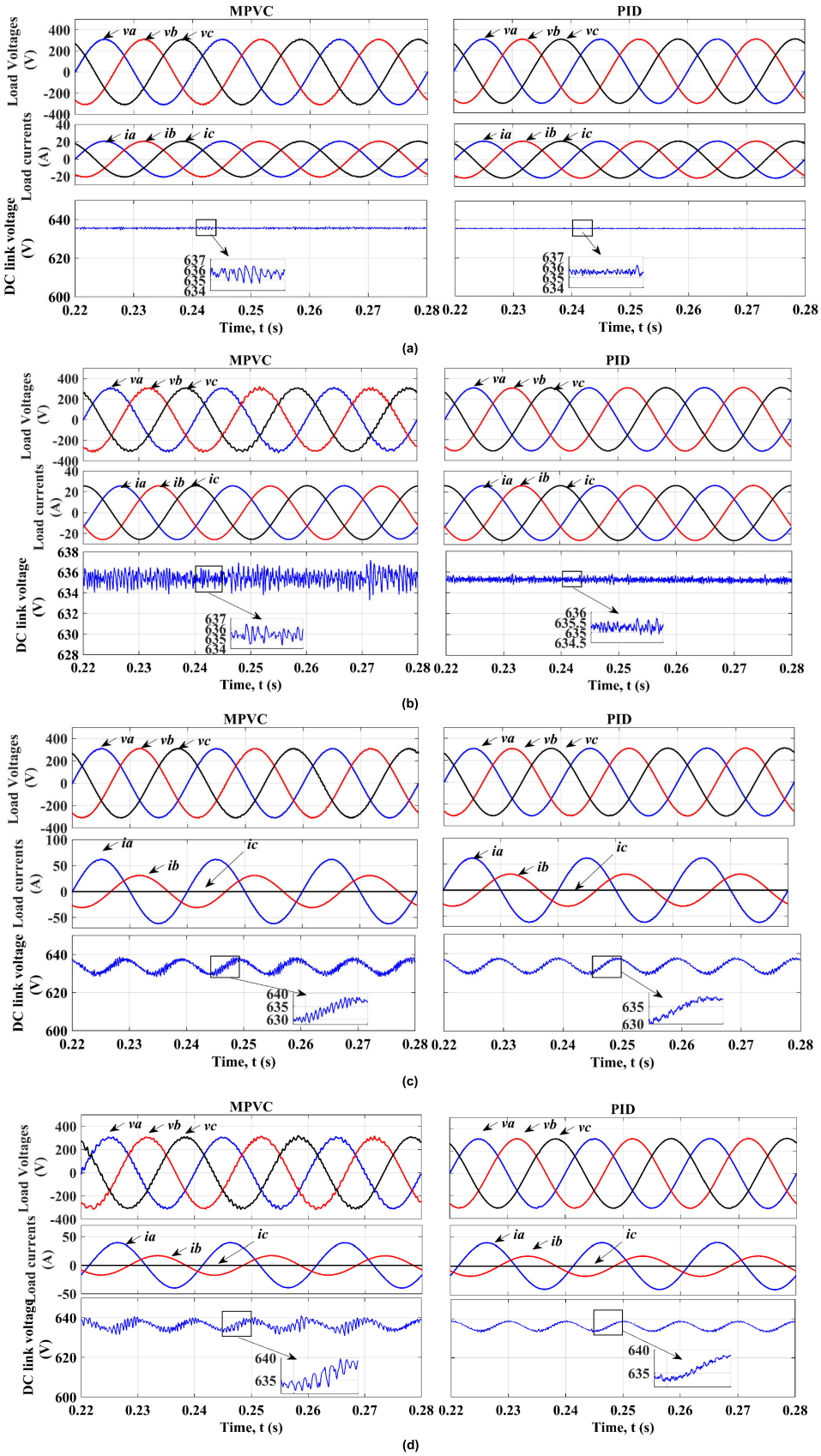

FIGURE 10. Load voltages, load currents, and DC-link voltage of APS under (a) load case 1 (b) load case 2 (c) load case 3 (d) load case 4 (e) load case 5.

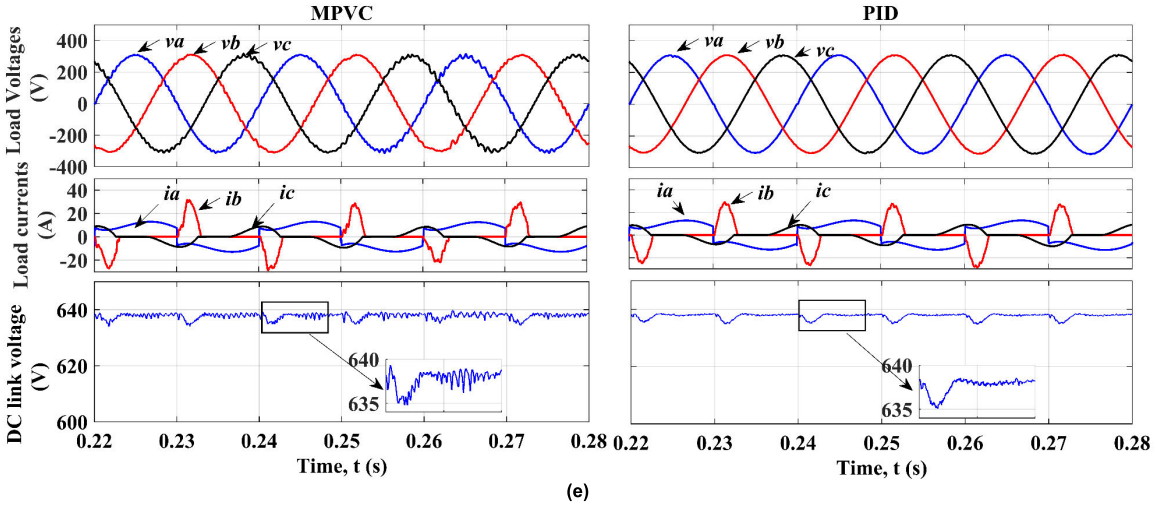

FIGURE 10. *(Continued.)* **Load voltages, load currents, and DC-link voltage of APS under (a) load case 1 (b) load case 2 (c) load case 3 (d) load case 4 (e) load case 5.**

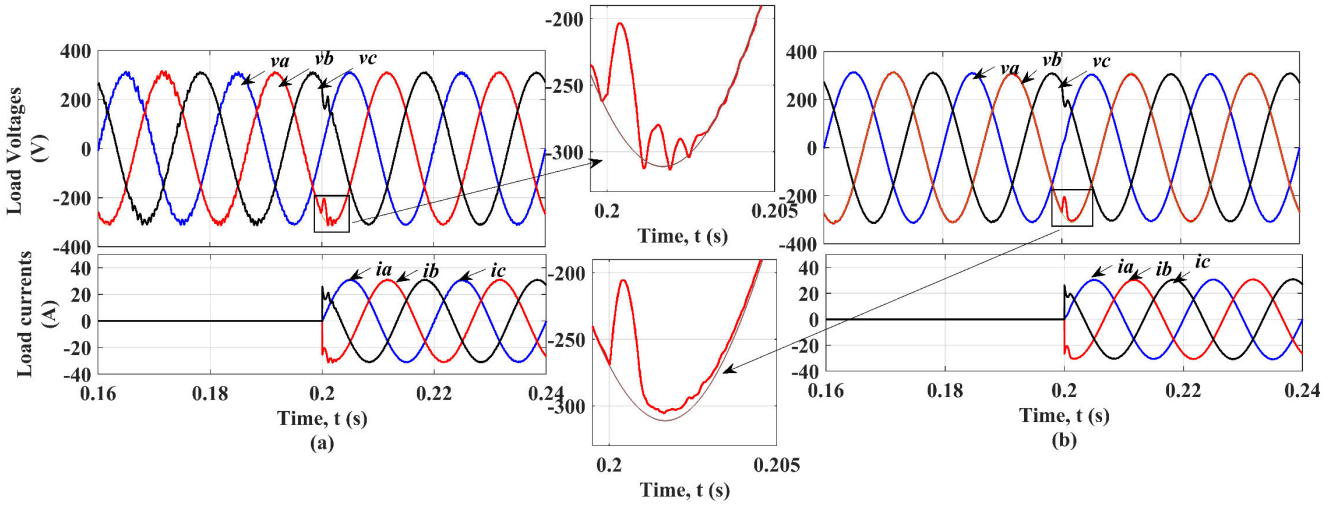

FIGURE 11. **Voltage and load currents of APS in the transient mode of (a) MPVC and (b) PID control.**

High f_s leads to high switching losses of the inverter and overheat. Furthermore, the high variation of f_s makes the design and choice of the LC-filter more complex. However, the MPVC operates with a variable f_s. The f_s is limited by the sampling time, as shown in Fig. 13, and does not exceed 5500 Hz in resistive and inductive loads. Fig. 13 shows the variation of f_s with the change in load power and power factor. In case of resistive load condition, with increasing the load demand, the f_s increases abruptly but is limited to a value of 5500 Hz. The f_s is limited by the sampling frequency because the control algorithm is repeated at each sampling period. The f_s is calculated for each switch by calculating the number of repeating changes in the SS of the switch for one second, and then the average f_s is chosen [38].

As the predictive model control depends mainly on the LC-filter parameters, two operating conditions are considered in the robustness test against LC-filter variation:

- CF: changing the filter parameters while the system model is not changed. In this case, the mismatch is presented between the actual parameters and the model parameters.
- CCF: changing the filter parameters and accordingly changing the system model at the same time.

Fig. 14a and 14b show the %THD of MPVC under LC-filter parameters variations in CF and CCF modes, respectively. In the case of CF, the %THD surface is lower than 5%, and the mean value of the THD variation is 2.0288% which is very close to the mean value of the % THD in CCF mode which is 1.1156%. The same test is applied to PID control as shown in Fig. 14c. The %THD surface of PID is

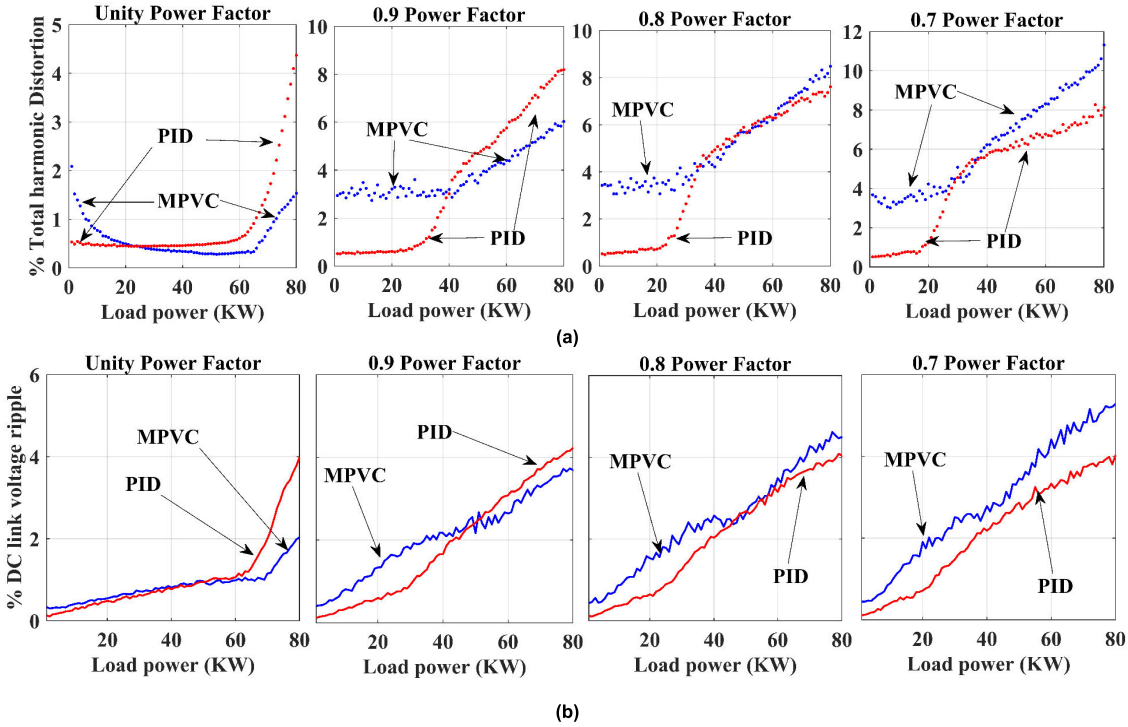

FIGURE 12. The effect of load change on (a) %THD and (b)% ΔVdc.

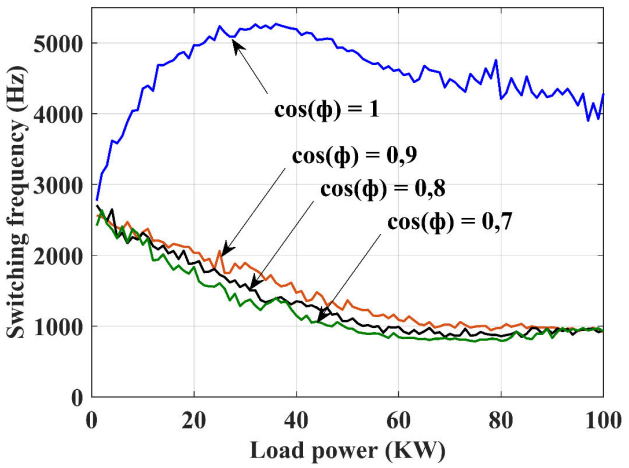

FIGURE 13. The f_s considering the load power and power factor variations.

located between the two surfaces of %THD of MPVC with a mean value of 1.4954%. The $\%\Delta V_{dc}$ for MPVC variation against the change of filter parameters in CF and CCF modes are shown in Fig. 15a and 15b, respectively, and for PID control in Fig. 15c. The filter parameters have little effect on MPVC and PID performance. From these analyses, it can be observed that the MPVC has good robustness against filters parameters variations, like PID controller, although it is a model-based control technique.

However, it is well known that the f_s of MPVC is limited by the sampling frequency due to the fact that the control algorithm is repeated at each sampling period. The following analyses are studied to show how the f_s is changing according to the LC filter parameters. The f_s variation of MPVC under changing LC filter parameters for CF and CCF modes are depicted in Fig. 16a and 16b, respectively. The f_s deviation from lower to higher LC filter parameters is from 1500 to 5500 Hz in CF case and from 3500 to 4500 Hz in CCF case. Therefore, the f_s variation in CCF mode is lower than that in CF mode by 75%. It can be highly observed that the variation in filter inductance has a less impact on the f_s than the filter capacitance variation.

VIII. EXPERIMENTAL RESULTS

To test MPVC experimentally, an APS project containing a three-phase FLVSI with an output LC filter has been built in the laboratory. The control algorithm is realized in the microprocessor module STM32F769BIT6 (216 MHz). The reference voltages are defined in the microcontroller memory. The current sensors LEM GAS 25-NP are used to provide the measured analog current signals for the microcontroller. Nine measuring channels are designed, Operational Amplifiers with analog low-pass filters, to scale the analog signals of currents and voltages according to the analog input ratings of the microcontroller. Considering the safety issues, the experiments are performed under low voltage level, the DC-link voltage is equal to 60 V and is provided by two 30 V power supplies connected in series. Therefore, the load voltage signals are directly sent to the measuring channels without using voltage transducers. The analog to digital converters are combined in the microcontroller integrated circuit.

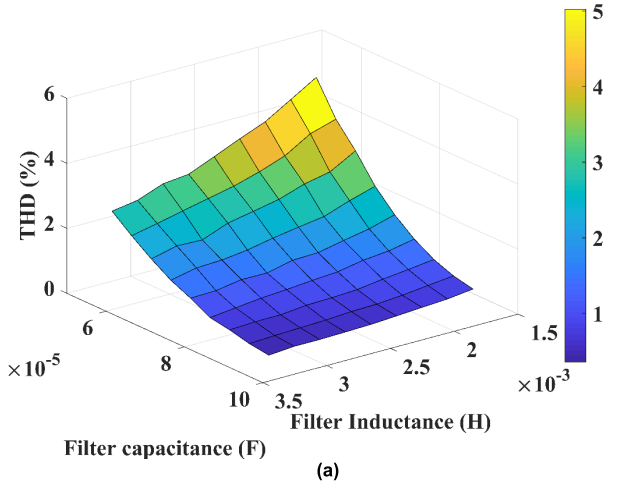

(a)

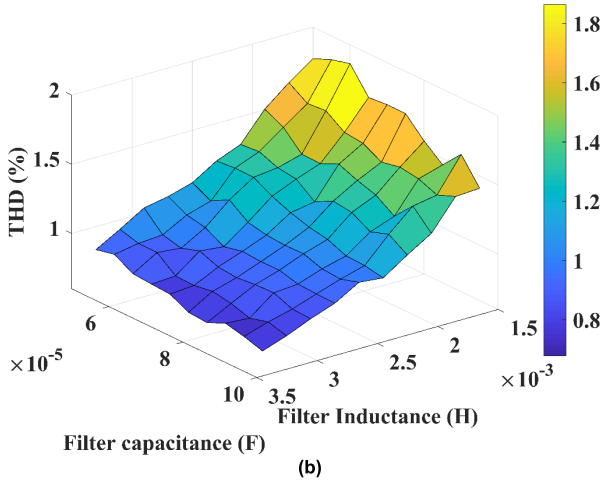

(b)

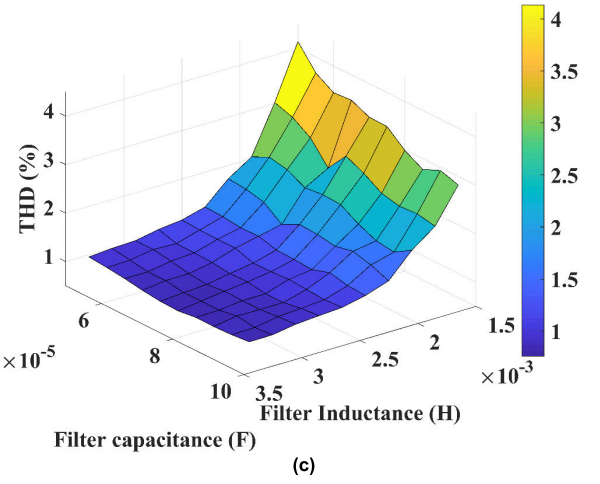

(c)

FIGURE 14. The %THD variation against the LC-filter parameters for (a) MPVC (CF), (b) MPVC (CCF), and (c) PID.

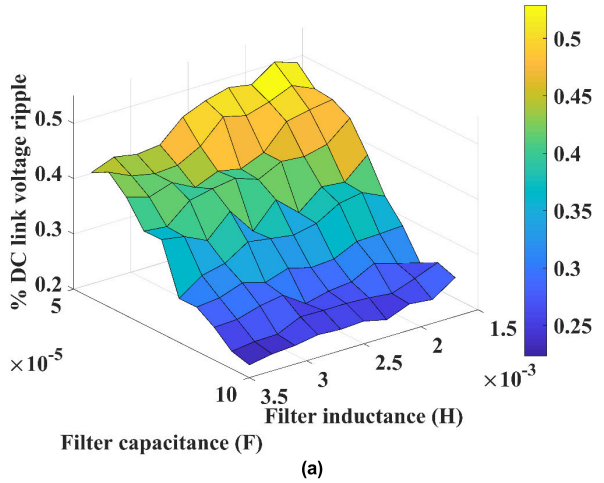

(a)

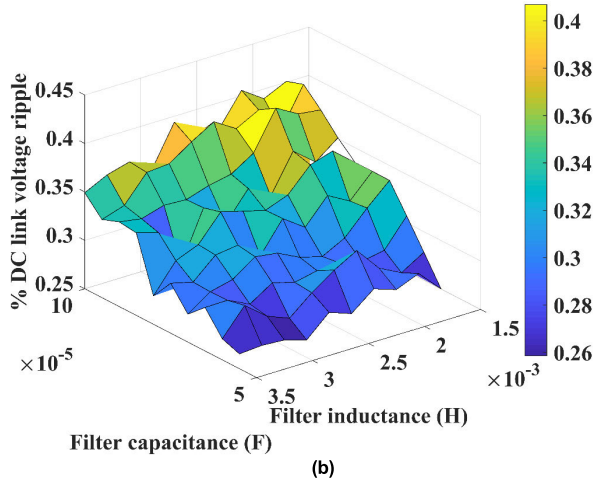

(b)

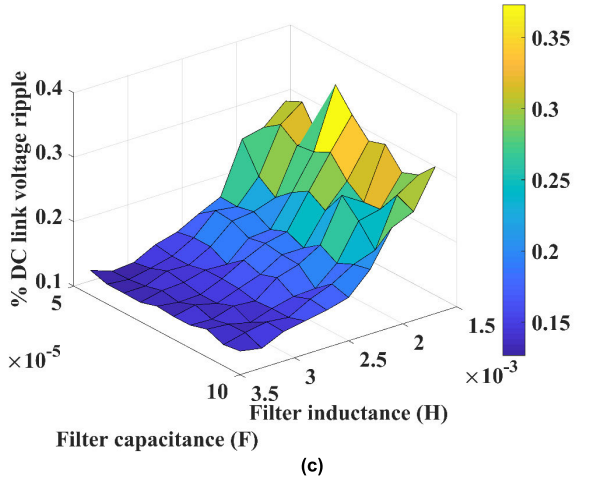

(c)

FIGURE 15. The % ΔV_{dc} variation against the LC-filter parameters for (a) MPVC (CF), (b) MPVC (CCF), and (c) PID.

The output signals from the microcontroller are sent to the switching devices (MOSFET IXFN110N60P3) through the Gate Drive Circuits. The waveforms of the three-phase load voltages and currents were displayed on a LeCroy Wave Runner oscilloscope. Another DC power supplies i used for supplying the measuring and control circuits. The parameters of the system are shown in Table 7. The real view and the schematic diagram of the developed project are shown in Fig. 17.

TABLE 6. Comparizon between FCS-MPC algorithms for computation effort reduction.

The proposed algorithm in:	*Ts* (µs)	CT (µs)	Inverter topology	Number of SS	Control platform
This paper	25	12.3	FLVSI	16	DSP STM32F769BIT6 (216 MHz)
[24]	33	14	Three-leg VSI	8	DSP TMS320F28335 (150 MHz)
[25]	83.3	24.2	T-type three-level VSI	27	DSP TMS320F28335 (150 MHz)
[26]	100	-----	Three-leg VSI	8	Simulink-Real-Time system
[27]	20	8	FLVSI	16	double-CPU: FPGA EP4CE115F23I7 (472.5 MHz) DSP TMS320F28335 (150 MHz)
[28]	30	---	Three-leg VSI	8	-----

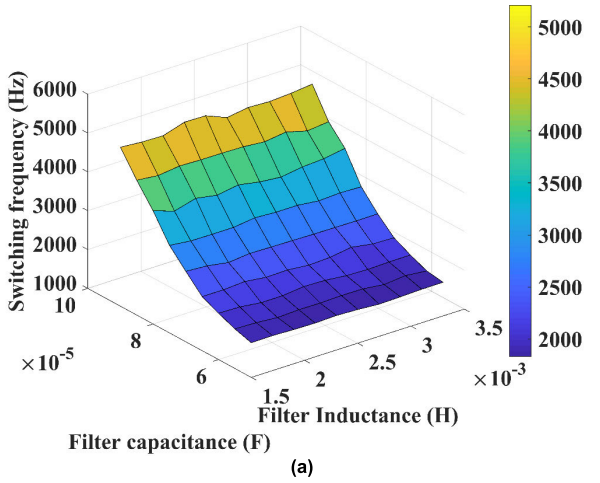

FIGURE 16. The f_s variation of MPVC against the LC-filter parameters in (a) CF case and (b) CCF case.

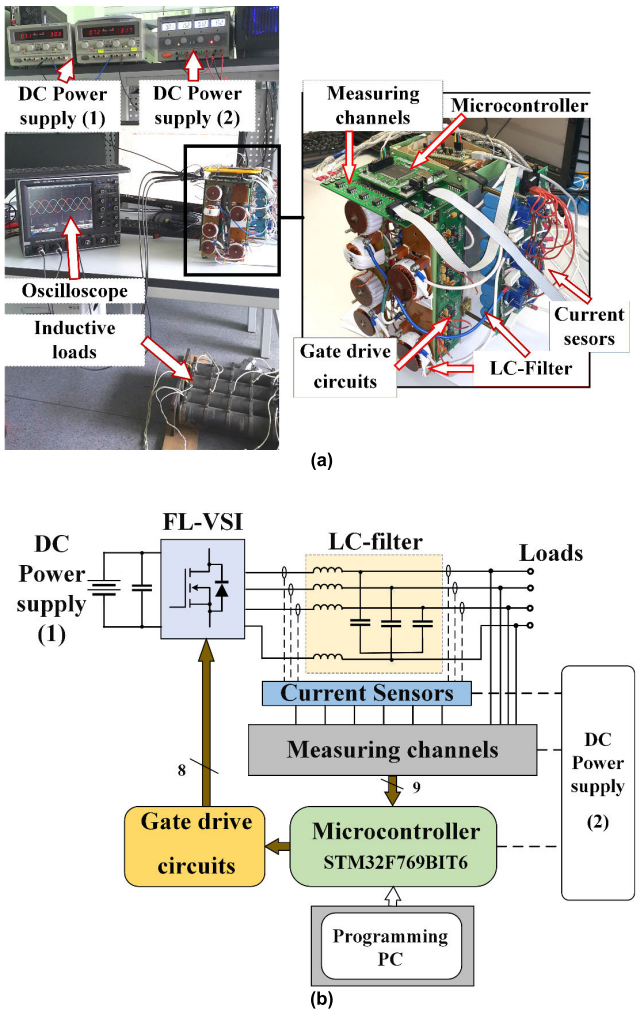

FIGURE 17. The experimental setup (a) real view (b) schematic diagram.

TABLE 7. Experimental parameters.

Parameters	Values
DC input power supply	V_{dc} = 60 V, Pdc = 720 Watt
Sampling time	T_s = 25 µs
DC-link capacitance	C_{dc} = 800 µF
LC filter	R = 0.1 Ω, L = 1 mH, C= 90 µF

Due to the time optimization performed for the proposed MPVC algorithm, the CT of MPVC is reduced from 28 μs to 12.3 μs with a reduction equal to 56%. This gives the opportunity to decrease the sampling time to its optimal value for the algorithm implementation. To select the best value of sampling time, the effect of sampling time on the control performance is analyzed and shown in Fig. 18. The switching frequency has an inverse relation with the sampling time, while the %THD has a proportional relation. It can be determined that the MPVC gives the best performance at $T_s = 25$ μs. If the T_s is lower than this value, the switching frequency will be greatly increased resulting in high switching loss and overheating. If T_s is higher than 25 μs,

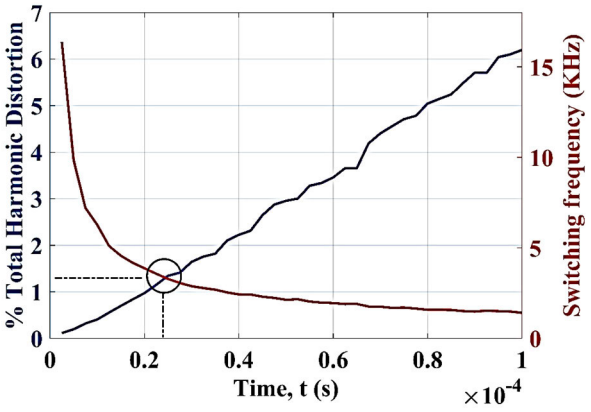

FIGURE 18. The effect of sampling time on the MPVC performance.

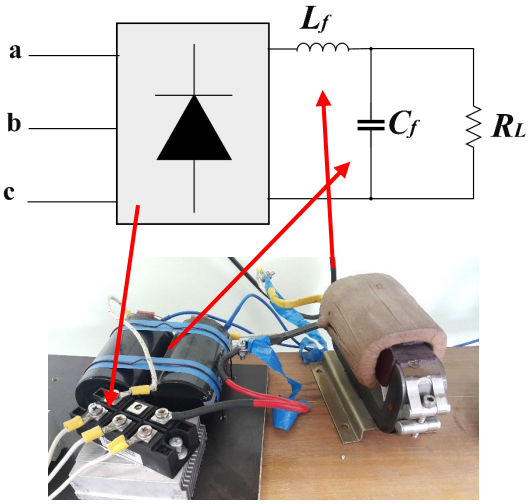

FIGURE 19. The topology of the three-phase nonlinear load and its experimental setup.

the f_s will be slightly decreased but the load voltage will be more distorted. Therefore, the sampling time selected for the algorithm implementation is ($T_s = 25\ \mu$s).

Table 6 shows the comparison between the proposed algorithm and the other FCS-MPC algorithms which are considering the CT reduction. It can be noted that, as the number of SS increases the algorithm requires longer CT. With increasing the microprocessor speed, the CT decreases. From Table 6, it can be determined that the CT of the proposed algorithm is lower even than the algorithms which are applied for the 8-SS three-leg VSI. However, the microprocessor in [27] is about three times faster than the available one in this work. The CT of the proposed algorithm is comparable with that in [27].

Three case studies are performed to assure the effectiveness of the MPVC algorithm in steady state operation with:

1- Unbalanced inductive load ($R_a = 6\ \Omega$, $R_b = 9\ \Omega$, Rc = 12, $La = 2$ mH, $L_b = 3$ mH, $L_b = 4$ mH).
2- Non-linear load.
3- Resistive load step-change

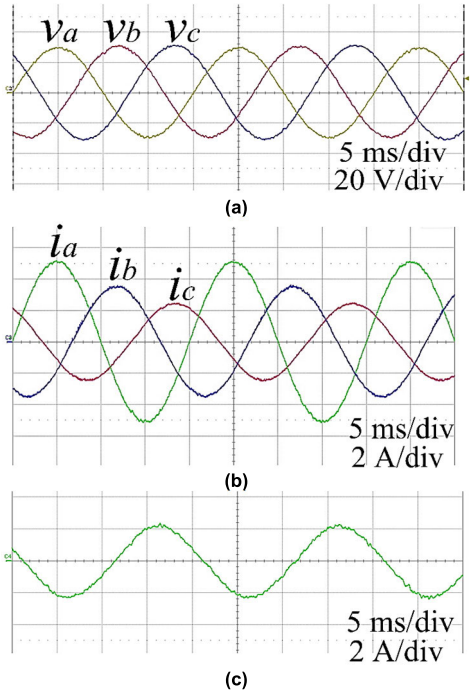

FIGURE 20. Experimental results in case of three-phase inductive load (a) load voltages (b) load currents (c) neutral current.

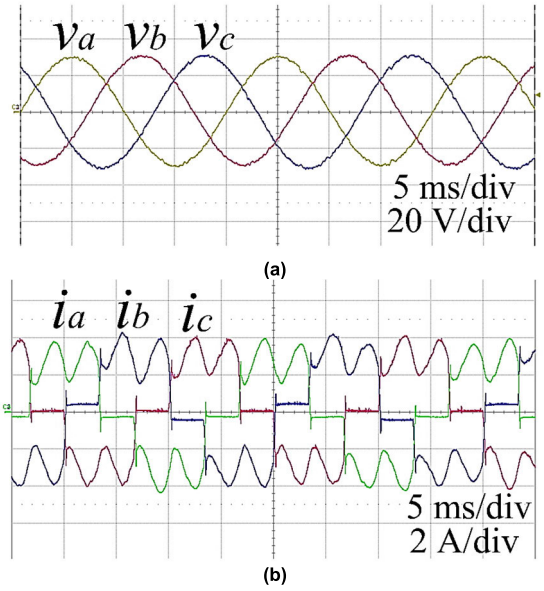

FIGURE 21. Experimental results in case of three-phase non-linear load (a) load voltages (b) load currents.

The nonlinear load available in the laboratory consists of resistive load with rectifier and LC-low-pass filter ($L_f = 1.3\ mH$, $C_f = 1400\ \mu$F, $R_a = 10\Omega$); the topology of this load is shown in Fig. 19.

The waveforms of load voltages, load currents and neutral current in case of the three-phase unbalanced inductive loads are shown in Fig.20a, Fig.20b and Fig.20c, respectively. The results show that the load voltages quite accurately follow the

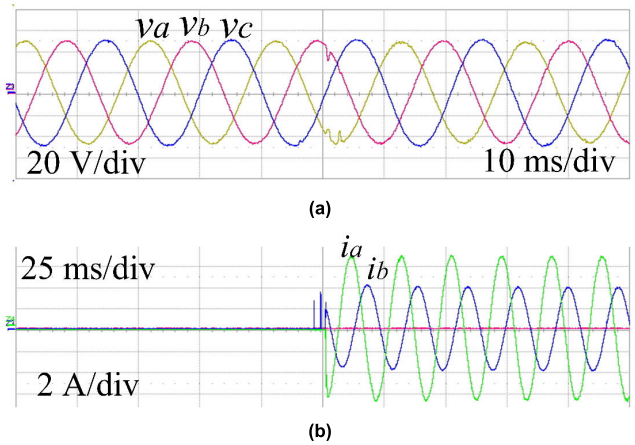

FIGURE 22. Experimental results under step-change (a) load voltages (b) load currents.

reference voltages with low distortion. As shown in Fig. 20b, the load currents are different and are determined by the total load demand of each individual phase; this causes the current to flow in the neutral wire as shown in Fig. 20c.

The experimental results which are shown in Fig. 21 confirm the abilityof the MPVC to handle the nonlinear loads. However, load currents are completely distorted due to the nonlinearity behavior of the load. The MPVC provides sinusoidal load voltage with very low harmonic distortion.

The transient test which is performed in the simulation section is repeated experimentally with an unbalanced resistive load ($R_a = 5\ \Omega$, $R_b = 10\Omega$, and $R_c = \infty$), see Fig. 22. The step-change is experimentally occurred by an automatic power switch. The experimental results assure the fast dynamic reaction of MPVC with a low overshoot level. The recovering time is about 3 ms and a voltage dip 10% of the peak value. It can be observed that spark may be provided in real switching, resulting in current pulses before closing the switching contacts completely. However, this phenomenon does not affect the load voltage which is robustly regulated by the proposed MPVC algorithm.

IX. CONCLUSION AND RECOMMENDATIONS

In this paper, MPVC is used to control the load voltage of FLVSI with output LC-filter in APS. An accurate discrete state-space model is presented, including the neutral line inductance and the damper resistance of the LC-filter. The performance of the MPVC is studied in a full comparative study with a PID-controller for voltage control of autonomous FLVSI. The advantages of MPVC technique can be pointed out as follows:

- The MPVC control scheme is simpler and consists of one control loop.
- The MPVC can operate in NRF and has more ability to control each phase independently.
- This control technique does not need parameter tuning in the designing procedure.
- The MPVC has a faster transient reaction.
- The MPVC provides lower distortion in the load voltage with resistive load.
- The %THD and $\%\Delta Vc$ have lower variation under the load change.
- The robustness of MPVC is high and comparable with the PID control.

The computation time required for the MPVC implementation is high, resulting in higher sampling time and lower performance of this control technique. In this paper, to reduce the CT required for the MPVC algorithm, a simple modification is performed to the MPVC algorithm to predict 15 voltage vectors instead of 16. The proposed MPVC algorithm is time optimized by removing the repeated and additional calculations without affecting the control performance. The CT is reduced by 56 % and the algorithm can be realized with a minimum sampling time of 25 μs for the available microprocessor.

The experimental results confirmed the simulation results that the proposed MPVC algorithm is able to handle unbalanced and nonlinear loads with high quality and fast transient response.

After an exhaustive research, it is determined that further research is recommended in the future work to discuss and resolve the following research issues of the FCS-MPC technique:

- Most of the FCS-MPC algorithms are proposed for the applications of the stand-alone inverters such as in stand-alone microgrids, Uninterruptible Power Supplies, and APSs, the power-sharing issues of the multi-inverter situation are not perfectly investigated in the literature.
- Future research should concentrate on the application of FCS-MPC as a hierarchical control of microgrids containing more than one inverter with considering the primary, secondary and tertiary control levels.
- More methods of time optimizations and reduction are required for the FCS-MPC algorithm to be effectively applied for multilevel inverters which have a large number of SSs and for the inverters which are used in 400 Hz power systems, such as aircrafts.

ACKNOWLEDGMENT

The development of the control systems was carried out at Tomsk Polytechnic University within the framework of Tomsk Polytechnic University Competitiveness Enhancement Program.

REFERENCES

[1] G. Zhang, Z. Li, B. Zhang, and W. A. Halang, "Power electronics converters: Past, present and future," *Renew. Sustain. Energy Rev.*, vol. 81, pp. 2028–2044, Jan. 2018.
[2] R. Aboelsaud, A. Ibrahim, and A. G. Garganeev, "Review of three-phase inverters control for unbalanced load compensation," *Int. J. Power Electron. Drive Syst.*, vol. 10, no. 1, pp. 242–255, 2019.
[3] R. M. Kamel, "New inverter control for balancing standalone micro-grid phase voltages: A review on MG power quality improvement," *Renew. Sustain. Energy Rev.*, vol. 63, pp. 520–532, Sep. 2016.

[4] F. Akter, K. S. Alam, and M. P. Akter, "Simplified model predictive control of four-leg inverters for stand-alone power systems," in *Proc. 10th Int. Conf. Electr. Comput. Eng. (ICECE)*, no. 3, Dec. 2018, pp. 261–264.

[5] A. G. Garganeev, R. Aboelsaud, and A. Ibrahim, "A novel predictive control algorithm for autonomous power supply systems," in *Proc. 4th Int. Conf. Frontiers Educ. Technol. (ICFET)*, 2018, pp. 170–175.

[6] Y. Song and B. Wang, "A hybrid electric vehicle powertrain with fault-tolerant capability," in *Proc. 27th Annu. IEEE Appl. Power Electron. Conf. Exposit. (APEC)*, Feb. 2012, pp. 951–956.

[7] M. Pichan, H. Rastegar, and M. Monfared, "A new digital control of four-leg inverters in the natural reference frame for renewable energy–based distributed generation," *Int. Trans. Electr. Energy Syst.*, Jul. 2018, pp. 1–18, Feb. 2019.

[8] A. M. Fahmy, A. K. Abdelslam, A. A. Lotfy, M. Hamad, and A. Kotb, "A four leg shunt active power filter predictive fuzzy logic controller for low-voltage unbalanced-load distribution networks," *J. Power Electron.*, vol. 18, no. 2, pp. 573–587, 2018.

[9] M. R. Miveh, M. F. Rahmat, M. W. Mustafa, A. A. Ghadimi, and A. Rezvani, "An improved control strategy for a four-leg grid-forming power converter under unbalanced load conditions," *Adv. Power Electron.*, vol. 2016, pp. 1–14, Aug. 2016.

[10] S. Vazquez, J. I. Leon, L. G. Franquelo, J. Rodriguez, H. A. Young, A. Marquez, and P. Zanchetta, "Model predictive control: A review of its applications in power electronics," *IEEE Ind. Electron. Mag.*, vol. 8, no. 1, pp. 16–31, Mar. 2014.

[11] S. Vazquez, J. Rodriguez, M. Rivera, L. G. Franquelo, and M. Norambuena, "Model predictive control for power converters and drives: Advances and trends," *IEEE Trans. Ind. Electron.*, vol. 64, no. 2, pp. 935–947, Feb. 2017.

[12] V. Yaramasu, M. Rivera, B. Wu, and J. Rodriguez, "Predictive control of four-leg power converters," in *Proc. IEEE Int. Symp. Predictive Control Electr. Drives Power Electron. (PRECEDE)*, Oct. 2015, pp. 121–125.

[13] V. Yaramasu, M. Rivera, M. Narimani, B. Wu, and J. Rodriguez, "Model predictive approach for a simple and effective load voltage control of four-leg inverter with an output *LC* filter," *IEEE Trans. Ind. Electron.*, vol. 61, no. 10, pp. 5259–5270, Oct. 2014.

[14] C. Zheng, T. Dragicevic, and F. Blaabjerg, "Current-sensorless finite-set model predictive control for LC-filtered voltage source inverters," *IEEE Trans. Power Electron.*, vol. 35, no. 1, pp. 1086–1095, Jan. 2020.

[15] C. Zheng, T. Dragicevic, B. Majmunovic, and F. Blaabjerg, "Constrained modulated model-predictive control of an LC-filtered voltage-source converter," *IEEE Trans. Power Electron.*, vol. 35, no. 2, pp. 1967–1977, Feb. 2020.

[16] K. Antoniewicz and M. Malinowski, "Comparison of current control strategies for four-leg shunt active power filter in Matlab-simulink," *Prz. Elektrotechniczny*, vol. 90, no. 10, pp. 214–218, 2014.

[17] V. K. Singh, R. N. Tripathi, and T. Hanamoto, "Comparative analysis of finite control set MPC for voltage source inverter," in *Proc. 5th Int. Conf. Electr. Power Energy Convers. Syst. (EPECS)*, Apr. 2018, pp. 1–6.

[18] H. A. Young, M. A. Perez, and J. Rodriguez, "Analysis of finite-control-set model predictive current control with model parameter mismatch in a three-phase inverter," *IEEE Trans. Ind. Electron.*, vol. 63, no. 5, pp. 3100–3107, May 2016.

[19] V. Yaramasu, J. Rodriguez, B. Wu, M. Rivera, A. Wilson, and C. Rojas, "A simple and effective solution for superior performance in two-level four-leg voltage source inverters: Predictive voltage control," *IEEE Int. Symp. Ind. Electron.*, Jul. 2010, pp. 3127–3132.

[20] H. T. Nguyen, J. Kim, and J.-W. Jung, "Improved model predictive control by robust prediction and stability-constrained finite states for three-phase inverters with an output *LC* filter," *IEEE Access*, vol. 7, pp. 12673–12685, 2019.

[21] T. Dragicevic, "Model predictive control of power converters for robust and fast operation of AC microgrids," *IEEE Trans. Power Electron.*, vol. 33, no. 7, pp. 6304–6317, Jul. 2018.

[22] F. Donoso, A. Mora, R. Cardenas, A. Angulo, D. Saez, and M. Rivera, "Finite-set model-predictive control strategies for a 3L-NPC inverter operating with fixed switching frequency," *IEEE Trans. Ind. Electron.*, vol. 65, no. 5, pp. 3954–3965, May 2018.

[23] B. Hu, L. Kang, J. Liu, J. Zeng, S. Wang, and Z. Zhang, "Model predictive direct power control with fixed switching frequency and computational amount reduction," *IEEE J. Emerg. Sel. Topics Power Electron.*, vol. 7, no. 2, pp. 956–966, Jun. 2019.

[24] C. Xia, S. Member, T. Liu, T. Shi, and Z. Song, "A simplified finite-control-set model-predictive control for power converters," *IEEE Trans. Ind. Informat.*, vol. 10, no. 2, pp. 991–1002, Oct. 2014.

[25] Y. Yang, H. Wen, M. Fan, M. Xie, and R. Chen, "Fast finite-switching-state model predictive control method without weighting factors for T-type three-level three-phase inverters," *IEEE Trans. Ind. Informat.*, vol. 15, no. 3, pp. 1298–1310, Mar. 2019.

[26] T. Jin, J. Guo, M. A. Mohamed, and M. Wang, "A novel model predictive control via optimized vector selection method for common-mode voltage reduction of three-phase inverters," *IEEE Access*, vol. 7, pp. 95351–95363, 2019.

[27] Q. Chen, X. Luo, L. Zhang, and S. Quan, "Model predictive control for three-phase four-leg grid-tied inverters," *IEEE Access*, vol. 5, pp. 2834–2841, 2017.

[28] I. S. Mohamed, S. Rovetta, T. D. Do, T. Dragicevic, and A. A. Z. Diab, "A neural-network-based model predictive control of three-phase inverter with an output *LC* filter," *IEEE Access*, vol. 7, pp. 124737–124749, 2019.

[29] M. Rivera, V. Yaramasu, J. Rodriguez, and B. Wu, "Model predictive current control of two-level four-leg inverters—Part II: Experimental implementation and validation," *IEEE Trans. Power Electron.*, vol. 28, no. 7, pp. 3469–3478, Jul. 2013.

[30] Z. Liu, J. Liu, and J. Li, "Modeling, analysis, and mitigation of load neutral point voltage for three-phase four-leg inverter," *IEEE Trans. Ind. Electron.*, vol. 60, no. 5, pp. 2010–2021, May 2013.

[31] M. Hojabri, M. Hojabri, and A. Toudeshki, "Passive damping filter design and application for three-phase PV grid-connected inverter," *Int. J. Trend Sci. Res. Develop.*, vol. 1, no. 6, pp. 346–348, Oct. 2017.

[32] R. Aboelsaud, A. Ibrahim, and A. G. Garganeev, "Voltage control of autonomous power supply systems based on PID controller under unbalanced and nonlinear load conditions," in *Proc. Int. Youth Conf. Radio Electron., Electr. Power Eng. (REEPE)*, Mar. 2019, pp. 1–6.

[33] M. P. Akter, S. Mekhilef, N. M. L. Tan, and H. Akagi, "Stability and performance investigations of model predictive controlled active-front-end (AFE) rectifiers for energy storage systems," *J. Power Electron.*, vol. 15, no. 1, pp. 202–215, Jan. 2015.

[34] M. Uddin, S. Mekhilef, and M. Rivera, "High performance modified model predictive control of a voltage source inverter," *Electr. Power Compon. Syst.*, vol. 46, no. 5, pp. 600–613, Mar. 2018.

[35] T.-H. Chen, C.-H. Yang, and N.-C. Yang, "Examination of the definitions of voltage unbalance," *Int. J. Electr. Power Energy Syst.*, vol. 49, no. 1, pp. 380–385, Jul. 2013.

[36] X. Lu and F. Zheng Peng, "Minimizing DC capacitor current ripple and DC capacitance requirement of the HEV converter/inverter systems," in *Proc. IEEE Energy Convers. Congr. Exposit.*, Sep. 2009, pp. 1191–1198.

[37] T. Jin, X. Shen, T. Su, and R. C. C. Flesch, "Model predictive voltage control based on finite control set with computation time delay compensation for PV systems," *IEEE Trans. Energy Convers.*, vol. 34, no. 1, pp. 330–338, Mar. 2019.

[38] J. Rodriguez and P. Cortes, *Predictive Control of Power Converters and Electrical Drives*. Hoboken, NJ, USA: Wiley, 2012.

RAEF ABOELSAUD was born in Zagazig, Egypt, in 1987. He received the B.Sc. degree (Hons.) and the M.Sc. degree in electrical engineering from Zagazig University, Zagazig, in 2009 and 2013, respectively. He is currently pursuing the Ph.D. degree with National Research Tomsk Polytechnic University, Tomsk, Russia. He is also a Teaching Assistant with the School of Energy and Power Engineering, Tomsk Polytechnic University. He has authored or coauthored over 20 research articles and papers that are published in high-impacted journals and conferences. His current research interests include power electronic converters and control systems applied to electric power grids and renewable energy systems.

AMEENA SAAD AL-SUMAITI received the B.Sc. degree in electrical engineering from United Arab Emirates University, United Arab Emirates, in 2008, and the M.A.Sc. and Ph.D. degrees in electrical and computer engineering from the University of Waterloo, Canada, in 2010 and 2015, respectively. She was a Visiting Assistant Professor with MIT, Cambridge, MA, USA, in 2017. She is currently an Assistant Professor with the Department of Electrical and Computer Engineering, Khalifa University, Abu Dhabi, United Arab Emirates. Her research interests include intelligent systems, energy economics, and energy policy.

AHMED IBRAHIM was born in El Sharkia, Egypt, in 1987. He received the B.Sc. and M.Sc. degrees from the Faculty of Engineering, Zagazig University, Egypt, in 2009 and 2013, respectively.

He is currently a Teaching Assistant with National Research Tomsk Polytechnic University, Tomsk, Russia. He is also working in the field of optimization techniques, control systems, electric power grids, and renewable energy systems. He has more than 22 research articles and papers that are published in high-impacted journals and conferences.

IVAN V. ALEXANDROV (Graduate Student Member, IEEE) was born in Novosibirsk, in 1996. He is currently pursuing the master's degree with the Radio Engineering and Electronics Faculty, Novosibirsk State Technical University (NSTU). His research interests include very high-frequency switching converters, dynamics analysis of power systems, and advanced PWM techniques.

ALEXANDER G. GARGANEEV received the degree in electrical equipment of aircrafts from Tomsk Polytechnic University, Tomsk, Russia, in 1978. He is the Head of the Department "Electro-technical complexes and materials" in scientific research, Tomsk Polytechnic University. He has 250 scientific publications in electric power engineering and electrical engineering. His current research interests include electric drives, power electronics, and process and industrial automation.

AHMED A. ZAKI DIAB received the B.Sc. and M.Sc. degrees in electrical engineering from Minia University, Egypt, in 2006 and 2009, respectively, and the Ph.D. degree from the Electric Drives and Industry Automation Department, Faculty of Mechatronics and Automation, Novosibirsk State Technical University, Novosibirsk, Russia, in 2015. He had obtained a Postdoctoral Fellowship with the Moscow Power Engineering Institute (MPEI) (National Research University), Moscow, Russia, from September 2017 to March 2018. Since 2007, he has been a Teaching Assistant and a Lecturer Assistant with the Department of Electrical Engineering, Faculty of Engineering, Minia University, where he has been an Assistant Professor, since 2015. He is currently a Visitor Researcher (Postdoctoral) with the Green Power Electronics Circuits Laboratory, Kyushu University, Japan (awarded the MIF Research Fellowship 2019, Japan). He is certified as a Siemens Engineer and a Trainer in several fields of automation and process control systems. He is also the Supervisor of the Automatic Control and Traction Laboratory, Faculty of Engineering, Minia University. His current research interests include renewable energy systems, power electronics, and machines drives.